metals

Article

Effect of Heat Treatment on Microstructure and Hardness of Grade 91 Steel

Triratna Shrestha [1], Sultan F. Alsagabi [1], Indrajit Charit [1], Gabriel P. Potirniche [2] and Michael V. Glazoff [3,*]

[1] Department of Chemical and Materials Engineering, University of Idaho, Moscow, ID 83844-3024, USA; E-Mails: triratna.shrestha@gmail.com (T.S.); ssagabi@kacst.edu.sa (S.F.A.); icharit@uidaho.edu (I.C.)

[2] Department of Mechanical Engineering, University of Idaho, Moscow, ID 83844-0902, USA; E-Mail: gabrielp@uidaho.edu

[3] Energy Systems Integration, Idaho National Laboratory, Idaho Falls, ID 83415-3710, USA

* Author to whom correspondence should be addressed; E-Mail: michael.glazoff@inl.gov; Tel.: +1-208-526-8937.

Abstract: Grade 91 steel (modified 9Cr-1Mo steel) is considered a prospective material for the Next Generation Nuclear Power Plant for application in reactor pressure vessels at temperatures of up to 650 °C. In this study, heat treatment of Grade 91 steel was performed by normalizing and tempering the steel at various temperatures for different periods of time. Optical microscopy, scanning and transmission electron microscopy in conjunction with microhardness profiles and calorimetric plots were used to understand the microstructural evolution including precipitate structures and were correlated with mechanical behavior of the steel. Thermo-Calc™ calculations were used to support the experimental work. Furthermore, carbon isopleth and temperature dependencies of the volume fraction of different precipitates were constructed.

Keywords: modified 9Cr-1Mo steel; Grade 91 steel; heat treatment; microstructure; differential scanning calorimetry; Thermo-Calc™; precipitates

1. Introduction

The Next Generation Nuclear Plant (NGNP) is expected to address the growing energy demand by producing electricity and, at the same time, mitigate greenhouse gas emissions by co-producing hydrogen from the process heat. The Very High Temperature Reactor (VHTR) is a Gen-IV reactor system at the heart of the NGNP. VHTRs are designed to operate at temperatures much higher than those of currently operating reactors. Moreover, they are designed for longer service periods (60 years or more) compared to the current operating reactors [1]. The operating temperature of the reactor pressure vessel (RPV) in VHTR can vary between 300 and 650 °C. Furthermore, the RPVs will be more than double the size of a typical RPV as found in a Light Water Reactor (LWR) [2].

The modified 9Cr-1Mo steel (Grade 91) is a material of choice in fossil-fuel-fired power plants with increased efficiency, service life, and reduction in emissions of CO_2, NO_x, and SO_2. The efficiency of fossil-fired power strongly depends on the temperature and pressure of steam. One percent increase in net efficiency reduced the emission of CO_2, NO_x, SO_2, and particulates by 2.4 metric ton, 2000 ton, 2000 ton, and 500 ton, respectively, while also reducing fuel costs by 2.4% [3]. Temperature of steam in coal-fired power plant is expected to be in the range of 550–720 °C and pressure is expected to be above 24 MPa [3–5].

Grade 91 steels are a ferritic-martensitic (F-M) class of steel with superior creep strength [6,7]. The addition of strong carbide and carbonitride formers like vanadium (V), niobium (Nb), and titanium (Ti) lead to the precipitation of various particles, such as $M_{23}C_6$, and MX type precipitates: (Ti,Nb)(N,C), (Nb,V)(C,N), and (V,Nb)(N,C). The smaller interparticle spacing and increased volume fraction of the fine MX carbides enhance the alloy strength. These precipitates obstruct the movement of dislocations, refine grains during normalizing, and delay plastic deformation [6,8]. However, precipitates like Z-phase and Laves phase may lead to a decrease in the strength of the alloy by weakening the solid solution.

Evolution of various precipitates and microstructure can be understood from the heat treatment, differential scanning calorimetric (DSC) studies, and thermodynamic calculations using Thermo-Calc. The heat treatment study of Grade 91 steel helps in understanding its microstructural evolution and mechanical properties; as this material, whether being used for a reactor pressure vessel or boiler component, goes through a series of heating, cooling, and welding processes. With the changes involved in normalizing and tempering temperatures, different types of carbides such as $M_{23}C_6$, Z-phase, Ti/Nb/V rich MX type carbide/carbonitrides precipitate and coarsen in Grade 91 steel resulting in a change in the creep strength, ductility, hardness, and microstructure. Ahn *et al.* [9] observed a decrease in the high temperature strength of an Nb containing steel due to coarsening of Nb-rich precipitates. DSC was used to measure the heat absorbed or liberated during heating or cooling associated with carbide precipitation and other phase changes. Ganesh *et al.* [10] were able to find the phase transformation temperatures including temperature ranges for dissolution of various precipitates in different low carbon steels.

The present article aims to elucidate the effects of various heat treatment conditions (normalizing and tempering) on Grade 91 steel. There are numerous studies on the normalizing/tempering of Grade 91 steel [11–15], but these studies are limited to few temperatures and times. Thus, this paper has taken about 50 normalizing and tempering conditions to study the relevant microstructural evolution.

To that end, a combination of microstructural characterization efforts and microhardness measurements was utilized. The findings were discussed with the help of DSC studies, and Thermo-Calc™ was used to understand the microstructural evolution and precipitate stability.

2. Experimental Details

2.1. Material

The manufacturer-supplied chemical composition of ASTM A387 Grade 91 CL2 steel used in this study is shown in Table 1. The hot rolled Grade 91 plates were obtained from American Alloy Steel, Houston, TX, USA, in a normalized and tempered condition (*i.e.*, austenitized at 1040 °C for 240 min followed by air cooling, and tempered at 790 °C for 43 min). The as-received plates were 10.4 cm × 10.4 cm × 1.27 cm in size. Heat treatment specimens were cut out from these plates using a diamond wafering blade. At room temperature, the as-received Grade 91 steel had an average yield strength of 533 MPa, ultimate tensile strength of 683 MPa and elongation to fracture of 19%.

Table 1. Chemical composition (in wt.%) of Grade 91 steel.

Element	Nominal	Measured
Cr	8.00–9.50	8.55
Mo	0.85–1.05	0.88
V	0.18–0.25	0.21
Nb	0.06–0.10	0.08
C	0.08–0.12	0.10
Mn	0.30–0.60	0.51
Cu	0.4 (max.)	0.18
Si	0.20–0.50	0.32
N	0.03–0.07	0.035
Ni	0.40 (max.)	0.15
P	0.02 (max.)	0.012
S	0.01 (max.)	0.005
Ti	0.01 (max.)	0.002
Al	0.02 (max.)	0.007
Zr	0.01 (max.)	0.001
Fe	Balance	Balance

2.2. Heat Treatment

Heat treatment was performed using an electric resistance furnace, capable of reaching a temperature exceeding 1200 °C. Normalizing was first done on each sample within a temperature range of 1020–1100 °C for 2, 4, and 8 h. Normalizing temperature and time were so chosen that austenitization had been complete before tempering was carried out. Normalized samples were air cooled down to room temperature before tempering at various temperatures and times. Samples that have been normalized at 1040 °C for 2, 4 and 8 h were tempered at 690, 725, 745 and 790 °C for 2, 8 and 20 h. Tempering of samples normalized at 1040 °C for 2 h was expanded to include temperatures in the range of 635–850 °C. This created a matrix of close to 50 possible combinations of normalizing and

tempering scenarios, which provided an adequate sequence to reveal the microstructural changes during heat treatment.

2.3. Metallographic Characterization

Optical microscopy was performed with Olympus optical microscope, Center Valley, PA, USA, on both the as-received and heat treated specimens for characterization of the grain structure. Optical micrographs were taken for each sample and provided visual representation of the changing phases and microstructural features. Transmission electron microscopy (TEM) studies were done on selected samples. Conventional metallographic procedures of cold mounting, grinding and polishing were followed to prepare the specimen surface to 0.5 μm finish before etching was carried out using Marble's reagent: A solution made of 50 mL distilled water, 50 mL hydrochloric acid and 10 g of copper sulfate. Subsequently, an Olympus light microscope, Center Valley, PA, USA was used to examine the metallographic specimens, and an attached CCD camera was used to record the images.

For the TEM study, the sectioned samples were mechanically polished down to ~120 μm thickness, and then 3 mm diameter disks were punched out of the samples. Those disks were then jet polished in Fischione twin-jet polisher using a solution of 80 volume% methanol and 20 volume% nitric acid solution at a temperature of about −40 °C. Dry ice bath was used to achieve low temperature. Philips CM200, San Francisco, CA, USA, and JEOL JEM-2010, Pleasanton, CA, USA, TEMs operated at an accelerating voltage of 200 kV were used to study in detail the grain and precipitate morphology of the material under both as-received and select heat treated conditions. The scope of the study did not involve extensive TEM study of these samples. The EDS system available in the same TEMs was used to estimate the chemical composition of precipitates. Hardness was measured using a Leco Vickers microhardness tester, St. Joseph, MI, USA; the applied load was 500 gf and the hold time was 15 s.

2.4. Thermodynamic Modeling

The calculations of thermodynamic equilibrium in Grade 91 steel and construction of C-isopleths were done with the help of Thermo-Calc AB software (Thermo-Calc Classic Version S, Stockholm, Sweden). Thermo-Calc TCFE6 database (Stockholm, Sweden) for iron-based alloys was used to conduct all the equilibrium calculations. Due to the significant complexity of the Grade 91 steel (iron plus 13 alloying elements), impurities such as S or P were excluded from the thermodynamic calculations.

2.5. Differential Scanning Calorimetry

Differential scanning calorimetric study of Grade 91 steel was done using a Netzsch STA 409 PC calorimeter, San Francisco, CA, USA. The DSC chamber was evacuated and purged several times with the argon gas of high purity (99.999%), and the flow rate of argon was maintained at 85 cm^3/min. The sample mass ranging between 50 and 60 mg was found suitable for an acceptable signal to noise ratio. The sensitivity curves for scan rate of 20 °C/min were calibrated using the melting point of pure indium, tin, zinc, aluminum and gold under research grade argon atmosphere. Baseline calibrations were performed by using a pair of empty crucibles corresponding to the heating rate of 20 °C/min. Non-isothermal

DSC measurements were done by heating the sample from 25 to 1400 °C, and then cooling was undertaken at the same rate down to 200 °C.

3. Results

3.1. Microstructural Characteristics

The as-received Grade 91 steel had a tempered martensitic microstructure with a lot of precipitates, as shown in Figure 1a,b. Precipitation hardening is one of the main strengthening mechanisms in highly alloyed steels like Grade 91. Alloying elements, such as C, N, Ti, Nb, V, Cr and Mo, promote the formation of precipitates like Cr-rich $M_{23}C_6$, and Ti or Nb or V-rich MX particles, where M stands for metals, *i.e.*, Cr, Mo, Ti, Nb or V. The Cr-rich $M_{23}C_6$ precipitates were elongated rod-like or block-like particles, while Ti-rich, Nb-rich and V-rich MX precipitates had nearly spherical shape. The Cr-rich $M_{23}C_6$ type precipitates were mainly observed at the lath boundaries and prior austenite grain boundaries (PAGB). The dimension of the elongated rod-like and block-like Cr-rich precipitates was measured, and found to have an average length of 285 ± 80 nm and width of 121 ± 39 nm, which is similar to that reported by Shen *et al.* [16] in 11Cr F-M steel and Anderson *et al.* [17] in Grade 91 steel. The average diameter of near-spherical MX-type precipitates was 37 ± 15 nm, similar to values reported in literature [3,16]. These types of precipitates were mainly located in the matrix and martensitic lath structure. These thermally stable fine precipitates enhance the long term creep resistance by impeding movement of mobile dislocations, prior austenite grain boundaries, martensite lath and subgrain boundaries, and restrict fine grain structure from recrystallization. For a constant normalizing time of 2 h, prior austenite grain size and martensite lath size increased with increasing normalizing temperatures of 1020 °C–1100 °C, as shown in Figure 2a–d. The as-normalized (1040 °C for 2 h) microstructure had hard martensitic lath structures with high dislocation density, as observed in Figure 2c,d. Similarly, for constant normalizing temperature of 1040 °C, martensite lath size and prior austenite grain size increased with increasing normalizing time of 2, 4 and 8 h. Figure 2e and f shows the optical and TEM micrograph of sample normalized at 1040 °C for 8 h, respectively. Figure 2g shows the EDS spectrum of a $M_{23}C_6$ type precipitate shown in Figure 2f, indicating the presence of Cr.
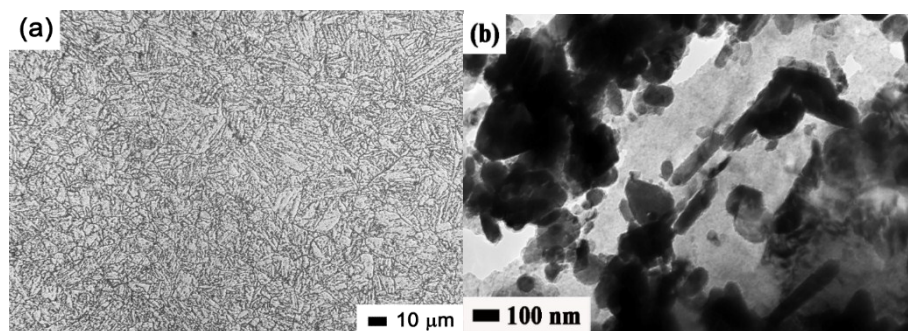

Figure 1. As-received microstructure: (**a**) optical and (**b**) TEM micrograph.
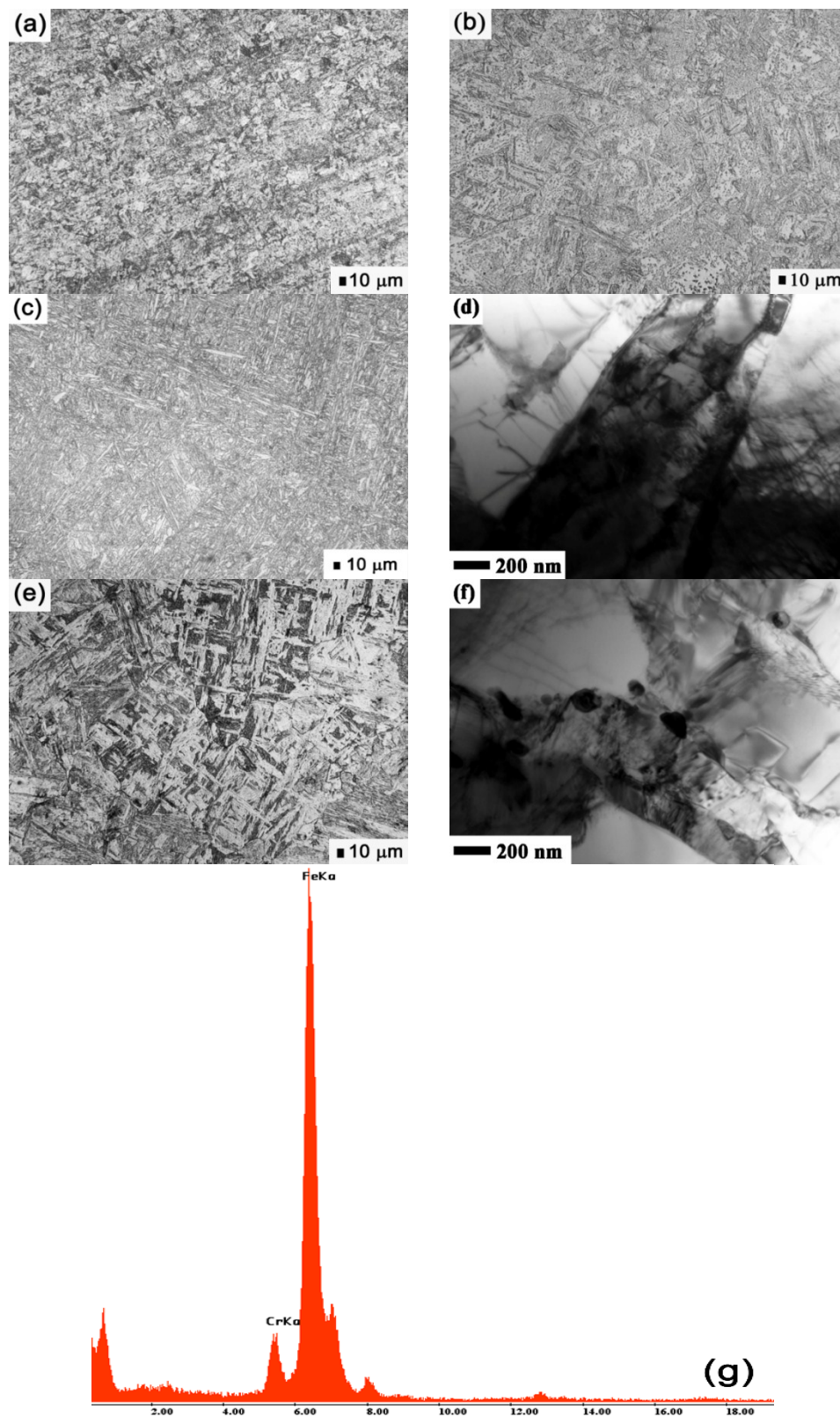
Figure 2. As-normalized optical micrograph (**a**) normalized at 1020 °C for 2 h; (**b**) normalized at 1100 °C for 2 h; (**c**) normalized at 1040 °C for 2 h; (**d**) TEM micrograph of sample normalized at 1040 °C for 2 h; (**e**) optical micrograph of sample normalized at 1040 °C for 8 h; (**f**) TEM micrograph of a sample normalized at 1040 °C for 8 h; and (**g**) the EDS spectrum of $M_{23}C_6$ type precipitate shown in Figure 2f.

The tempered microstructure of Grade 91 steel is shown in Figure 3. Figure 3a shows fine microstructure of sample normalized at 1040 °C for 2 h and tempered for 690 °C. Figure 3b shows coarse martensitic microstructure of sample normalized at 1040 °C for 2 h tempered at 745 °C for 8 h. Figure 3c and d shows the martensitic lath structure of sample normalized at 1040 °C for 2 h and tempered at 790 °C for 2 h. Grain size increased with increasing normalizing time, and tempering time. The sample normalized at 1040 °C for 2 h and tempered at 790 °C for 2 h has grain size of ~11 μm, while sample normalized at 1040 °C for 8 h and tempered at 790 °C for 20 h resulted in a grain size of ~17 μm. Figure 3e shows tempered martensitic structure of sample normalized at 1040 °C for 4 h and tempered at 725 °C for 2 h. Sample normalized at 1040 °C for 8 h and tempered at 790 °C for 20 h had coarse grain structure, as shown in Figure 3f.
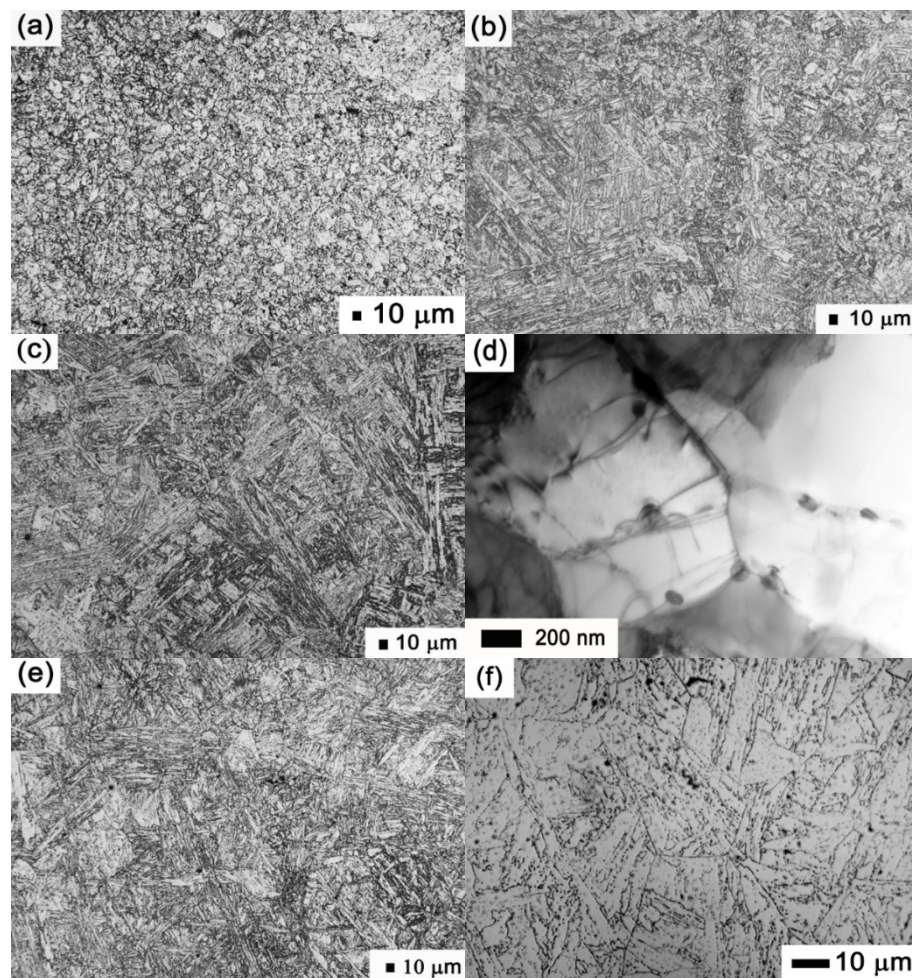
Figure 3. Tempered optical micrographs: (**a**) normalized at 1040 °C for 2 h and tempered at 690 °C for 2 h; (**b**) normalized at 1040 °C for 2 h and tempered at 745 °C for 8 h; (**c**) normalized at 1040 °C for 2 h and tempered at 790 °C for 2 h; (**d**) TEM micrograph of sample normalized at 1040 °C for 2 h and tempered at 790 °C for 2 h; optical micrographs (**e**) normalized at 1040 °C for 4 h and tempered at 725 °C for 2 h; and (**f**) normalized at 1040 °C for 8 h and tempered at 790 °C for 20 h.

3.2. Hardness of Heat Treated Steel

Normalizing treatment is intended for austenitization and homogenization of the solid solution. However, the right combination of normalizing temperature and time has to be found to optimize the material mechanical properties. Hardness measurements were performed on the alloy samples normalized at 1020, 1040, 1050, 1060, 1080 and 1100 °C while keeping the time constant at 2 h. The hardness decreased with increasing normalizing temperature, as shown in Figure 4a. The hardness value was about the same for normalizing carried out at 1020 and 1040 °C, but after that, the hardness gradually decreased until reaching 1100 °C. The effect of change in normalizing time was studied by heat treating Grade 91 steel at 1040 °C for 2 h, 4 h and 8 h. The hardness of the alloy decreased with increasing normalizing time, as shown in Figure 4b.

Alloy normalized at 1040 °C for 2 h was tempered at 690, 725, 745 and 790 °C for 2 h, 8 h and 20 h. Hardness of the alloy decreased with increasing tempering temperature and time, as shown in Figure 4c. Alloy tempered at 690 and 725 °C showed significant drop in hardness with increasing tempering time, but for 745 and 790 °C the decrease in hardness was gradual. Similar profiles were observed for samples normalized at 1040 °C for 4 h then tempered, and samples normalized at 1040 °C for 8 h then tempered at aforementioned temperatures, as shown in Figure 4d,e, respectively. Figure 4g shows the hardness of all tempered samples. Among all samples normalized at 1040 °C and tempered, samples normalized for 2 h and tempered at 690 °C for 2 h had the highest hardness, while sample normalized for 8 h and tempered at 790 °C for 20 h had the lowest hardness. The tempering temperature of the sample normalized at 1040 °C for 2 h was expanded to temperatures slightly above A_{C1} temperatures. Hardness of the alloy normalized at 1040 °C for 2 h and tempered for 2 h decreased with increasing tempering temperature up to 745 °C, stabilized till 820 °C, then increased, as shown in Figure 4f. Tempering above A_{C1} temperature was done to study the role of re-precipitation in Grade 91 steel.

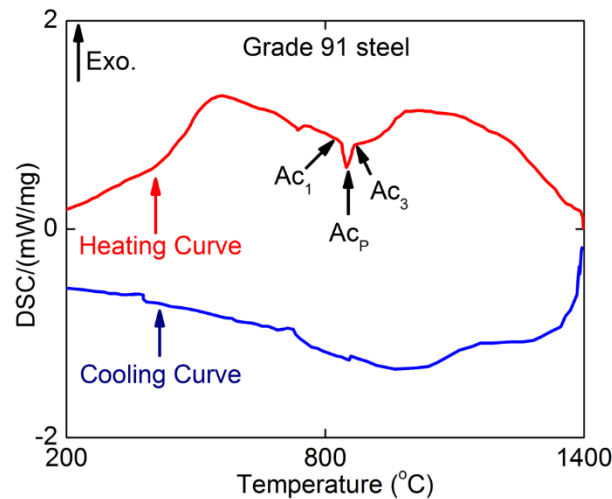### 3.3. Differential Scanning Calorimetry

Phase transformations of as-received (normalized and tempered) Grade 91 steel were studied using DSC. The phase transformations and reactions associated with heating and cooling of the alloy, as shown in Figure 5, are listed in Table 2. The listed temperatures for phase transformation and precipitate in Table 2 were obtained from the DSC curves, particularly with the help of its derivative in which inflection points are noticeably defined. The nature of the transformations was primarily corroborated by the Thermo-Calc calculations. The transformation of martensite to ferrite started at 550 °C, and the Curie temperature (T_c) signifying the change in ferromagnetic property was observed at 741 °C. The austenite phase started to form at 820 °C (A_{C1}), peaked at 848 °C (A_{Cp}), and the transformation was complete at 870 °C (A_{C3}), which was confirmed by differential thermal analysis (DTA) and the results of our thermodynamic calculations. The dissolution of $M_{23}C_6$ precipitate was complete at 870 °C. Dissolution of (V,Nb)(N,C) type precipitates bottomed out at 998 °C, but beyond that temperature they re-precipitated out. With the help of the first derivative of the heating curve, the onset of the second dissolution reaction of fine (V,Nb)(N,C) type precipitates was found to be at ~1140 °C. From cooling curve and its first derivative, the martensite start temperature (M_s) was calculated as 380 °C. Using A_{C1} as the onset temperature and A_{C3} as the end temperature, the DSC plot

was used to calculate the enthalpy associated with the α-*ferrite→austenite* phase transformation. The phase transformation enthalpy ($\Delta^{\circ}H^{\alpha \rightarrow \gamma}$) of 10 J/g was calculated.
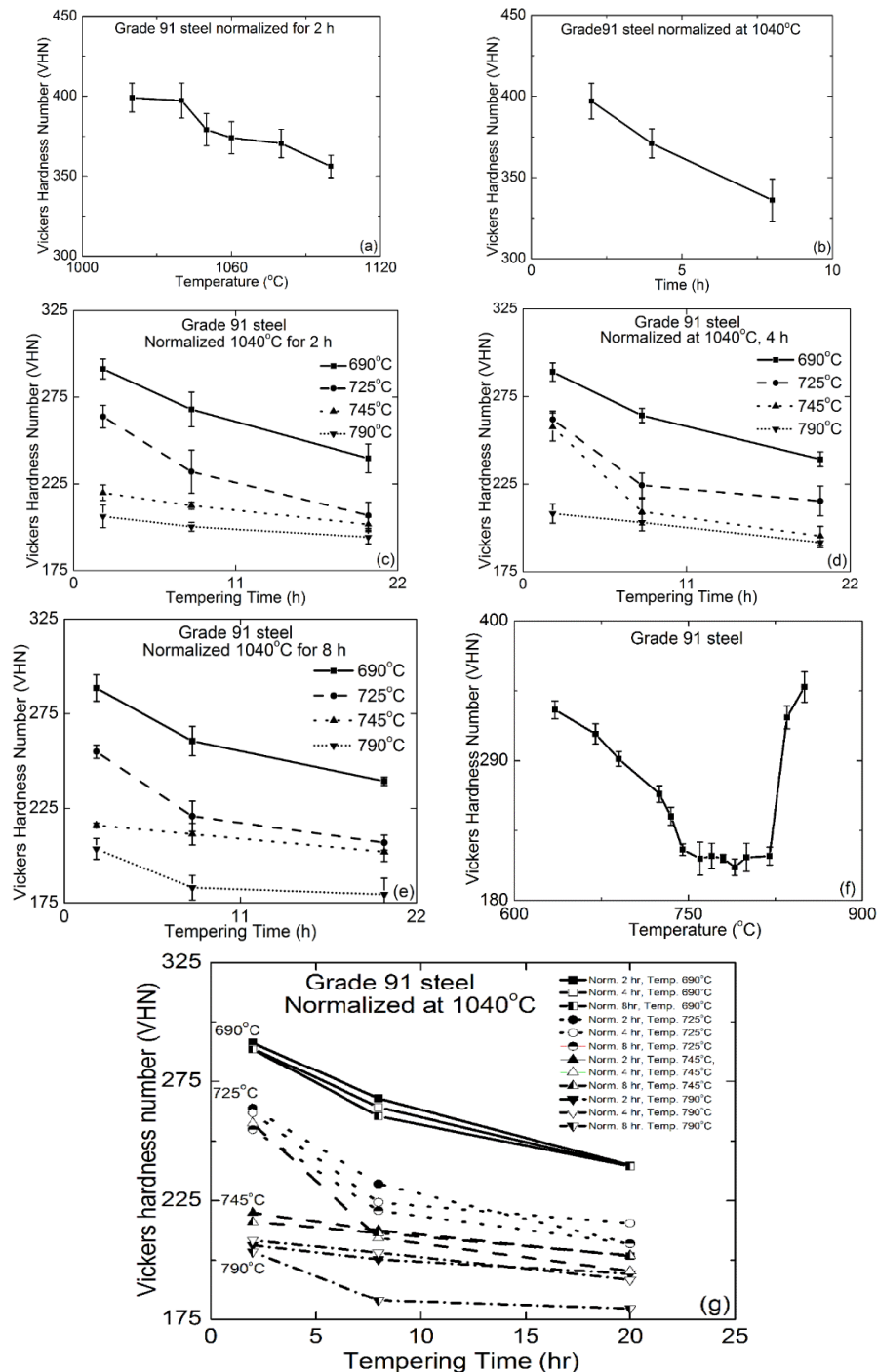
Figure 4. Variation in Vickers microhardness for various heat treatment conditions. (**a**) Variation in normalizing temperature; (**b**) samples normalized at 1040 °C for various times; (**c**) variation with tempering temperature and time for sample normalized at 1040 °C for 2 h; (**d**) Variation with tempering temperature and time for sample normalized at 1040 °C for 4 h; (**e**) variation with tempering temperature and time for sample normalized at 1040 °C for 8 h; (**f**) sample normalized at 1040 °C for 2 h and tempered at various temperatures for 2 h; and (**g**) normalized at 1040 °C and tempered samples.

Figure 5. Differential scanning calorimetric plot of as-received Grade 91 steel.

Table 2. Various transformation temperatures of Grade 91 steel.

| Description of Phase Change	Temperature (°C)
$\alpha' + M_{23}C_6 + (V,Nb)(N,C) + Z\text{-phase} \rightarrow \alpha + M_{23}C_6 + (V,Nb)(N,C) + Z\text{-phase}$	550
T_c (Curie Temperature)	741
$\alpha + M_{23}C_6 + (V,Nb)(N,C) + Z\text{-phase} \rightarrow \alpha + M_{23}C_6 + (V,Nb)(N,C) + (Nb,V)(C,N)$	770
$\alpha + M_{23}C_6 + (V,Nb)(N,C) + (Nb,V)(C,N) \rightarrow \alpha + \gamma + (V,Nb)(N,C) + (Nb,V)(C,N) + M_{23}C_6$	820 (A_{c1})
$\alpha + \gamma + (V,Nb)(N,C) + (Nb,V)(C,N) + M_{23}C_6 \rightarrow \gamma + (V,Nb)(N,C) + (Nb,V)(C,N)$	870 (A_{c3})
$\gamma + (V,Nb)(N,C) + (Nb,V)(C,N) \rightarrow \gamma + (Ti,Nb)(N,C) + (Nb,V)(C,N)$	1045
$\gamma + (Ti,Nb)(N,C) + (Nb,V)(C,N) \rightarrow \delta + \gamma + (Ti,Nb)(N,C)$	1270
$\delta + \gamma + (Ti,Nb)(N,C) \rightarrow \gamma + \delta$	1397
Martensite start (M_s)	380

3.4. Thermo-Calc Calculations

The carbon isopleth for the Fe-Cr-Mn-Mo-Nb-Ni-Ti-V-N-C full system is shown in Figure 6a. It is a property diagram, which represents the analog of the binary Fe-C phase diagram, but constructed for the full alloy system. It was calculated using the previously mentioned TCFE6 thermodynamic database. The bcc ferrite phase starts dissolving at ~810 °C and exists up to ~855 °C and then reappears above 1270 °C, as noted in Table 2. In between 850 and 1270 °C, the fcc austenite phase becomes stable. Other phases that are featured in the diagram in Figure 6a–c are the Z-phase; the $M_{23}C_6$-phase; (with metal M being mostly Cr); the Ti-rich (Ti,Nb)(N,C) precipitates; the Nb-rich and the Nb-poor (Nb,V)(C,N) precipitates; and the V-rich (V,Nb)(N,C) precipitates. All of the four phases have variable compositions but the same fcc crystalline lattice. The following notation was adopted for the latter four phases: In those cases when there was more carbon than nitrogen on a particular sublattice, the (C,N) notation was used; in the opposite case, the (N,C) notation was used. Similarly, the first position on the metal sublattice is assigned to a chemical element the concentration of which is the highest, e.g., (Nb,V); in the opposite case, the (V,Nb) notation was used.
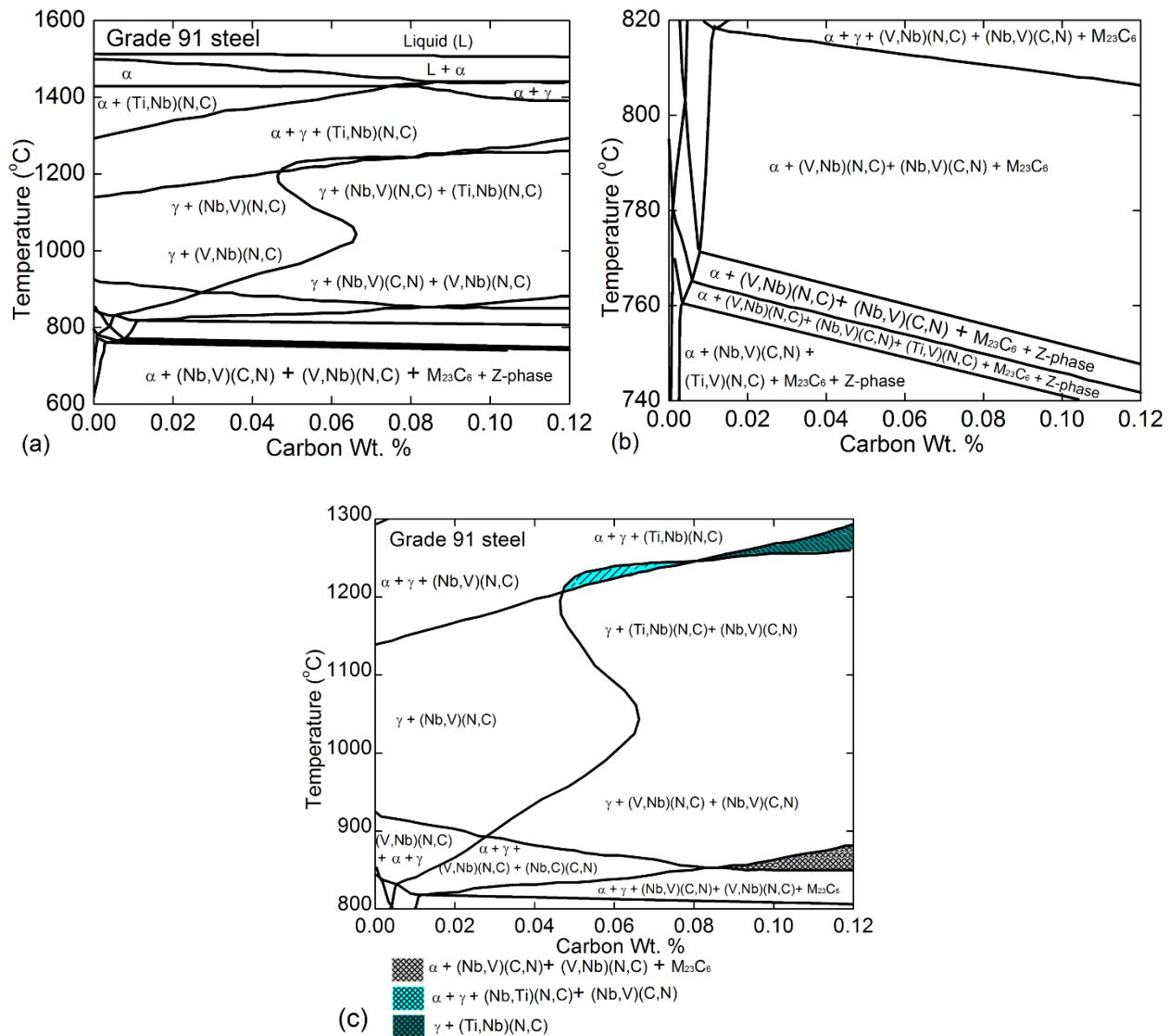
Figure 6. Carbon isopleth for Grade 91 steel. (**a**) Complete diagram: 600–1600 °C; (**b**) 740–820 °C; (**c**) 800–1300 °C.

It was established that the Ti-bearing precipitates (Ti,Nb)(C,N) were more stable than the (Nb,V)(C,N), and (V,Nb)(N,C) precipitates in the higher temperature range. Figure 7a shows a TEM micrograph of the as-normalized (normalized at 1040 °C for 2 h) sample with Ti-rich MX precipitates. The EDS spectrum of the Ti-MX particle is shown in Figure 7b. This example demonstrates the significance of simulations for the computational thermodynamics driven alloy design.

The evolution of the ferrite phase and its volume fraction with respect to temperature is shown in Figure 8a, and the evolution of $M_{23}C_6$ precipitate is shown in Figure 8b. The volume fraction of Z-phase, (Nb,V)(N,C) + (Ti,Nb)(N,C), and (V,Nb)(N,C) precipitates are illustrated by Figure 8c,d. Thermo-Calc calculations predicted that the volume fraction of $M_{23}C_6$ precipitate was higher than that of V-rich and Nb-rich MX type precipitates, owing to the higher wt.% of Cr and Mo compared to Nb and V. Higher resolution plot of the evolution of (V,Nb)(N,C) precipitate is shown in Figure 8d. Special attention was paid to the possibility of a phase separation and/or atomic clustering. Indeed, phase separation reaction and the miscibility gap were observed for the Fe-Cr system, so this possibility could not be excluded for the Fe-9Cr-1Mo steel.
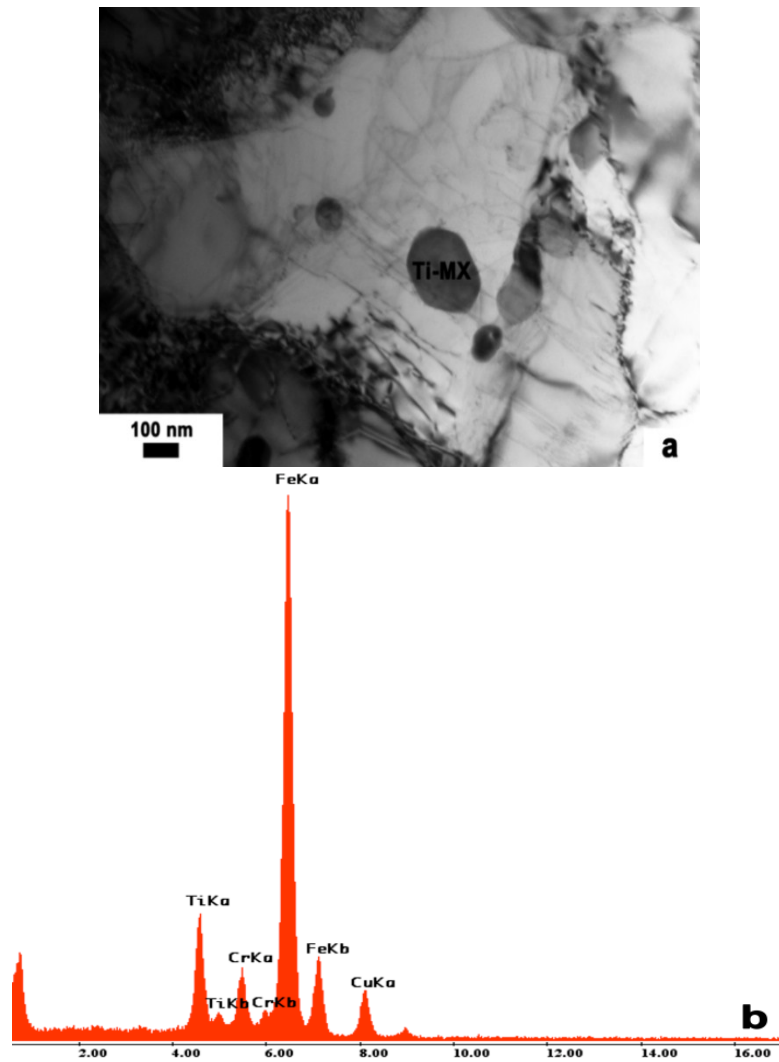
Figure 7. (**a**) A TEM micrograph of as-normalized (at 1040 °C for 2 h) sample; and (**b**) EDS of a Ti-rich MX precipitate.

4. Discussion

4.1. As-Normalized Microstructure

Hardness of the Grade 91 steel normalized for 2 h at 1020, 1040, 1050, 1060, 1080 and 1100 °C decreased with increasing temperature. Similarly, hardness of the as-normalized sample at 1040 °C decreased with increasing normalizing time. As-normalized microstructure had hard martensitic lath structures with high dislocation density, as shown in Figure 2d. Yoshino *et al.* [11] and Das *et al.* [18] reported increase in the prior austenite grain size with increase in normalizing temperatures from 1050 to 1250 °C. However, hardness remained constant in the same temperature range. However, in the current study, for normalizing carried out for 2 h in the temperature range of 1020–1100 °C, hardness decreased with increasing normalizing temperature. The decrease in the hardness value and increase in prior austenite grain size was due to a decrease in the volume fraction of precipitates with increased normalizing temperature and time. Average diameter of MX precipitates increased from 35 nm after normalizing at 1050 °C to 315 nm after normalizing at 1200 °C [11], leading to a decrease in the number density of precipitates.
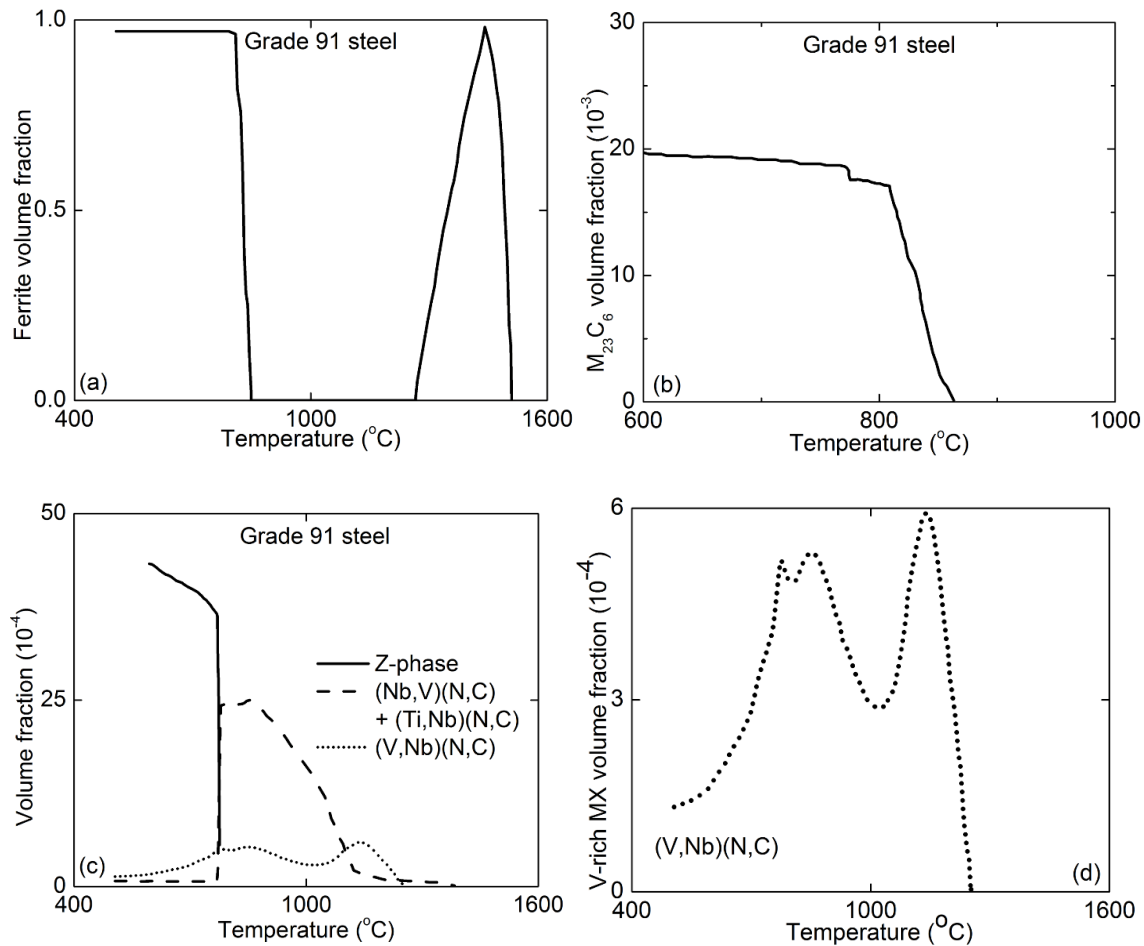
Figure 8. Evolutions of (**a**) the ferrite phase; (**b**) $M_{23}C_6$ precipitate; (**c**) Z-phase, Nb-rich MX, V-rich MX, and Ti-rich MX precipitates; and (**d**) high resolution plot of (V,Nb)(N,C) precipitate as a function of temperature.

Given the higher carbon solubility in austenite than in alpha ferrite, carbide precipitates dissolve in austenite. With increased diffusion at a higher temperature and longer time, the precipitates coarsen while the lath size and grain size also increase. Grade 91 steel normalized at 1040 °C for 8 h had a martensitic lath width of 473 ± 105 nm, and the size of the needle shaped $M_{23}C_6$ precipitates was 136 ± 75 nm in length and 28 ± 20 nm in width. While the sample normalized at 1040 °C for 2 h had a martensitic lath size of 335 ± 115 nm, while the $M_{23}C_6$ precipitates were 78 ± 15 nm in length and 13 ± 4 nm in width. At higher normalizing temperature, considerable grain growth occurred, but at lower normalizing temperature the austenite grain structure was finer. Moreover, normalizing below 900 °C resulted in partially transformed ferrite with patches of martensitic structure [12]. However, the change in the normalizing temperature in the range of 1020–1100 °C can result in different precipitate size distribution(s) that could possibly affect the mechanical behavior of the alloys.

4.2. Tempered Microstructure

The as-normalized hard martensitic lath structure with high dislocation density changed to stress-free, relaxed tempered martensitic structure upon tempering. Upon tempering, the normalized steel is reheated to a temperature just below Ac_1, which relieves stress in martensitic structure via carbon

diffusion and carbide formation. With increased tempering time, the diffusion of carbon is increased and simultaneously became stress relieved. For example, a P92 steel normalized at 1050 °C showed a decrease in hardness with increasing tempering temperature from 525 up to 720 °C. Similarly, the tensile strength and yield strength decreased with increasing tempering temperature [13]. Moreover, for Grade 91 steel tempered at 765, 730, and 680 °C, specimens tempered at the lowest temperature had the highest creep strength at 600 °C, as shown by Sawada *et al.* [14]. Tempering above Ac_1 temperature decreased the toughness of the material due to the formation of fresh martensite as found by Silwal *et al.* [19]. In the present work, the hardness decreased with increasing tempering temperature till Ac_1 temperature (820 °C). The decrease in hardness, as seen in Figure 4g, is due to the coarsening of precipitates, dissolution of $M_{23}C_6$ carbides, and breakdown of martensitic lath structure.

Coarser precipitates are not effective in impeding the mobility of dislocations, and affect the strength of the steel [6]. Decrease in hardness with increased temperature can also in part be associated with the increased molybdenum in carbides. In Fe-Mo-C steels tempered at 700 °C, Shtansky and Inden [20] observed 4% increase in the molybdenum content in $M_{23}C_6$ precipitates after increasing the tempering time from 25 to 500 h. Increased molybdenum content in precipitates implies removal of Mo from the matrix, thus weakening the solid solution. Moreover, the $M_{23}C_6$ precipitates located on the prior austenite grain boundaries penetrate into the grains with increasing tempering time. The stability of hardness at temperatures around 800 °C reflects the maximum precipitation rate for 0.1 wt.% C in the alloy. However, above 820 °C, the hardness increased because of secondary hardening resulting from increased volume fraction of (V,Nb)(N,C) and (Nb,V)(N,C) precipitates, as noted in Figure 8c for the respective precipitates. The tempered microstructure still consisted of precipitates and subgrain structures but with reduced dislocation density, as seen in Figure 3d. MX type precipitates were observed inside the subgrain structure and martensite lath structure. $M_{23}C_6$ precipitates were mainly located on the prior austenite grain boundaries and martensitic lath boundaries. The microstructure of Grade 91 steel tempered at the lowest temperature had much finer martensite lath size and higher dislocation density. The as-received material had a prior austenitic grain size of ~11 μm, while that of the sample normalized at 1040 °C for 8 h and tempered at 790 °C for 20 h was 17 μm. The martensitic lath size increased and dislocation density decreased upon tempering. Dudko *et al.* [13] noted that when tempered at 720 °C for 3 h, the lath size increased to 300 nm from 250 nm, and the dislocation density decreased to 6.2×10^{14} m^{-2} from 7.0×10^{14} m^{-2} compared to the as-normalized microstructure. In 9%–12% Cr heat resistant steels, the dislocation density, hardness, and creep rupture life were generally reduced, but ductility and subgrain size increased with increasing tempering temperature [3].

The transformation of martensite to alpha-ferrite is dependent on the tempering temperature and holding time. The tempering temperature and holding time of tempering can be described by a single empirical parameter known as the Hollomon-Jaffe parameter (P)

$$P = T\,(C + \log t) \tag{1}$$

where T (K) is temperature, C (40) constant, and t (s) time. Generally, in the Hollomon-Jaffe parameter, 20 is used as the constant (C), but in this study C (40) gave the best fit. Figure 9 shows the Hollomon-Jaffe parameter for Grade 91 steel normalized at 1040 °C/2 h, and tempered in the temperature range of 635–820 °C for 2, 8 and 20 h. Figure 9 can be used to describe the variation of hardness in the tempered Grade 91 steel as a function of tempering temperature/time (as shown in

Figures 3 and 4). In the plot in Figure 9, two distinct regions could be observed: A region with a steep decrease in hardness with increasing Hollomon-Jaffe parameter followed by a region where the hardness did not vary much. The lower Hollomon-Jaffe parameter signifies lower tempering temperature/time where microstructural evolution takes place gradually and did not achieve quite the equilibrium microstructure. However, at higher Hollomon-Jaffe parameter the microstructure achieves close-to-equilibrium structure and the microstructural parameters did not change so much to affect hardness to an appreciable extent. Figure 8 shows the Thermo-Calc calculations indicating a decrease in the volume fraction of precipitates around Ac_1 temperature. The data related to tempering condition above Ac_1 have not been included in Figure 9 as the Hollomon-Jaffe parameter does not apply to heat treatment above Ac_1 temperature.
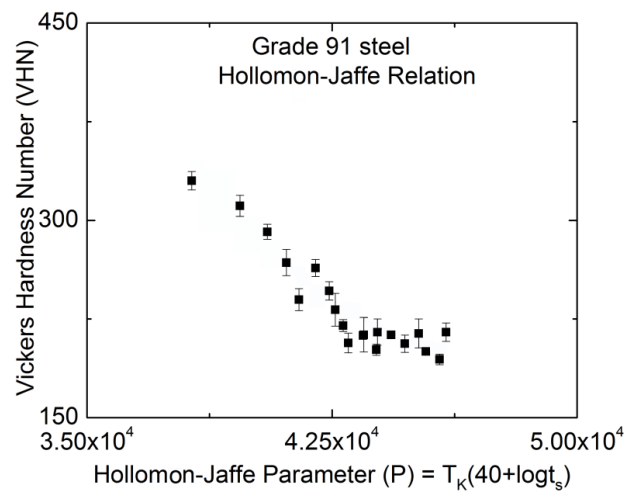
Figure 9. Hollomon-Jaffe relation of Grade 91 steel normalized at 1040 °C for 2 h and tempered at various temperatures and times.

4.3. DSC Study

The DSC plot shown in Figure 5 tracked the phase changes and reactions happening during heating and cooling of Grade 91 steel. Various temperatures associated with phase changes and reactions are listed in Table 2. DSC plot can slightly change depending on the heat treatment history of the material. Masuyama [15] reported that for various tempering temperatures, Ac_1 temperature was between 820 and 851 °C and the martensite transformation was ~400 °C. In this study, the Ac_1 temperature was 820 °C and the M_s temperature was 380 °C. DSC study of Grade 91 steel showed the change in the enthalpy associated with α-ferrite to austenite phase transformation is dependent on the starting microstructure produced by thermal aging [21]. A list of enthalpy change associated with α-ferrite to austenite phase transformation ($\Delta°H^{\alpha \to \gamma}$) is included in Table 3. The $\Delta°H^{\alpha \to \gamma}$ for or pure iron was 16 J·g^{-1}, but decreased with increased addition of alloying elements. Table 3 includes the enthalpy values of phase transformation (alpha-ferrite to austenite) for various steels. Substitutional solutes (such as W, Mo, V, Ti, Ta, Si) present in the steels in one or other combination are all ferrite-stabilizers. Even though steels contain carbon (an austenite stabilizer), the amount of C is fairly low. Thus, the addition of ferrite stabilizers to pure iron decreases the enthalpy, requiring more energy to transform to austenite and leading to a higher Ac_1/Ac_3 temperature. The volume fraction of (V,Nb)(C,N)

precipitates peaked initially at 790 °C and 850 °C, then started to dissolve in the matrix with the dissolution bottoming out at ~1000 °C and then peaked at ~1140 °C; these temperatures were captured with the help of the first derivative of the DSC heating curve. Furthermore, these temperatures were predicted by the Thermo-Calc calculations as shown in Figure 8c,d. The activation energy of Nb diffusion in the alpha-iron lattice is larger than those of Mo and Cr diffusion, and self-diffusion of iron [22]. Thus, the dissolution of Nb rich precipitates takes place at a higher temperature compared to the $M_{23}C_6$ precipitates. The MX type precipitates rich in V dissolve in the matrix before Nb, given the smaller atomic radius of V compared to Nb.

Table 3. Comparison of enthalpy associated with α→γ phase change.

Steel Composition (wt.%)	$\Delta^o H^{\alpha \to \gamma}$ (J·g^{-1})	Reference
Pure Iron	16	[21]
9Cr-1Mo	15	[10]
9Cr-1Mo-0.001V-0.1C	15	[21]
9Cr-1Mo-0.1C-0.42Si	13	[10]
9Cr-1W-0.23V-0.06Ta-0.1C	12	[23]
9Cr-1Mo-0.21V-0.08Nb-0.1C-0.002Ti	10	Present study

4.4. Thermo-Calc Calculations

In the present study, the normalizing temperatures (1020, 1040, 1050, 1060, 1080, and 1100 °C) and the temperature range of the subsequent tempering (690, 725, 745, and 790 °C) were of most interest. Figures 6 and 8 show the evolution of various phases as a function of temperature. These phase and precipitates play an important role in the formation of microstructure and strength of the heat treated alloy. The Thermo-Calc calculations predicted the existence of the Z-phase, but it was not observed in the TEM studies. During cooling, the austenite phase undergoes partial dissolution (the onset of transformation) at temperature ~850 °C and disappears completely at ~810 °C, in almost complete agreement with the findings of the DSC experiments (temperatures 870 and 820 °C, respectively). The Thermo-Calc does not make any distinction between α-ferrite and the δ-ferrite because they have the same bcc lattice. It would be appropriate to say that the α-ferrite dissolved at ~850 °C, but the δ-ferrite appeared at ~1270 °C peaked at ~1440 °C and then gradually dissolved as seen in Figure 8a.

The mass fraction of $M_{23}C_6$ precipitates remained constant up to the Ac_1 temperature but decreased drastically as austenite phase started forming. Given that austenite has higher affinity for C than α-ferrite, the $M_{23}C_6$ precipitates exist up to 865 °C, and then dissolve into the austenitic matrix. The mass fraction of MX type precipitates was constant till Ac_3 temperature, but then gradually decreased with increased temperature and totally dissolved at ~1200 °C [24]. In the present study, the volume fraction of Nb-rich MX increased at ~770 °C, started to decrease rapidly after ~850 °C, then gradually at ~1120 °C till 1260 °C. Since there was no clear distinction between the evolution of (Ti,Nb)(N,C) precipitate and (Nb,V)(N,C) precipitate, one could speculate that 1120 °C marks the onset of the phase separation reaction. As indicated in Figure 8c,d, the line indicating both (Nb,V)(N,C) and (Ti,Nb)(N,C) precipitates has a tail to it. The tail indicates the presence of Ti-rich MX which is stable up to ~1400 °C, as shown in Figure 6a. At around 470 °C, the dissolution of the M_6C precipitates was

observed in the Thermo-Calc calculations, not the Laves phase (absent at any temperature for x(C) = 0.001 wt.%). Laves phase was not observed in the as-received 9% Cr alloys containing 0.1% and 0.05% C with 0.03% Ti [3]. The Z-phase disappeared as the Nb-rich MX precipitates started to form. It remains to be established whether at such a low temperature there is enough time for the formation of such precipitates (M_6C). However, they were identified in the computed phase diagram quite reliably for different alloy compositions.

The temperature of 1045 °C corresponded to the terminus of the carbon solubility in the V-MX + Nb-MX phase field, as shown in Figure 6a. At this temperature range, a phase transformation reaction accompanied by the formation of the three types of Nb-bearing FCC precipitates: Nb-rich, V-rich and Ti-rich was obtained. Whether this could be considered as a transformation of the V-rich precipitates of the V-MX type (containing ~47 wt.% V and ~32% of Nb) into a new FCC phase in which the amounts of Nb and *V* are practically reversed, and the evolution of Ti-rich precipitate remains to be studied. Hong *et al.* [25] reported dendritic Nb-rich carbonitrides in high strength low alloy steel. On reheating the HSLA steel from 1050 to 1400 °C, the Nb content decreased with increasing temperature till 1250 °C. However, eventually, Ti started to dissolve into the austenite phase after 1300 °C. A similar observation was made in Grade 91 steel where the (Ti,Nb)(N,C) precipitate was stable at higher temperature compared to (Nb,V)(C,N) and (V,Nb)(N,C) precipitates. The solubility of (V,Nb)(C,N) was higher than that of (Ti,Nb)(C,N) and (Nb,Ti)(C,N) in both ferrite and austenite phases [26].

5. Conclusions

The heat treatment study of Grade 91 steel was performed, and Thermo-Calc calculations were used to predict the stability of various phases and provide guidance for future research in this direction. The hardness of the alloy decreased with increasing normalizing and tempering temperatures and times. The decrease in hardness was attributed to increase in the grain size, martensite lath size, and decrease in dislocation density and precipitate coarsening. Differential scanning calorimetry indicated the various phase changes and precipitate reactions taking place during heating and cooling of Grade 91 steel. The Thermo-Calc predicted the evolution of ferrite and austenite phases, and various precipitates. With the help of differential scanning calorimetry study and Thermo-Calc, various temperatures important to heat treatment of Grade 91 steel were identified. Normalizing of Grade 91 steel should be carried out in the temperature range of 1040–1270 °C, and tempering in the temperature range of 745–820 °C. Specific tempering optimization was not feasible in this study since only hardness was evaluated without any measurement of ductility and other relevant properties.

Author Contributions

Triratna Shrestha carried out experiments under Indrajit Charit and Gabriel P. Potirniche's guidance. Michael V. Glazoff performed the ThermoCalc calculations under Indrajit Charit and Triratna Shrestha's guidance. Data analyses were done in collaboration and characterization were done by Triratna Shrestha and Sultan F. Alsagabi.

Conflicts of Interest

The authors declare no conflict of interest.

References

1. Charit, I.; Murty, K.L. Structural materials issues for the next generation fission reactors. *JOM* **2010**, *62*, 67–74.
2. Murty, K.L.; Charit, I. Structural materials for Gen-IV nuclear reactors: Challenges and opportunities. *J. Nucl. Mater.* **2008**, *383*, 189–195.
3. Rojas, D. 9%–12% Cr Heat Resistant Steels: Alloy Design, Tem Characterization of Microstructure Evolution and Creep Response at 650 °C. Ph.D. Thesis, Ruhr-University Bochum, North Rhine-Westphalia, Germany, 2011.
4. Vishwanathan, R.; Bakker, W.T. Materials for boilers in ultra-supercritical power plants. In Proceedings of the 2000 International Joint Power Generation Conference, Miami Beach, FL, USA, 23–26 July 2000; pp. 1–22.
5. Buhre, B.J.P.; Gupta, R.; Richardson, S.; Sharma, A.; Spero, C.; Wall, T. PF-Fired supercritical boilers: Operational issues and coal quality impacts. Available online: http://www.steamforum.com/pictures/Supercritical%20TN%2020%20PF%20Super%20Critical.pdf (accessed on 20 January 2015).
6. Shrestha, T.; Basirat, M.; Charit, I.; Potirniche, G.P.; Rink, K.K. Creep deformation mechanisms in modified 9Cr-1Mo steel. *J. Nucl. Mater.* **2012**, *423*, 110–119.
7. Basirat, M.; Shrestha, T.; Potirniche, G.P.; Charit, I.; Rink, K. A study of the creep behavior of modified 9Cr-1Mo steel using continuum damage modeling. *Int. J. Plast.* **2012**, *37*, 95–107.
8. Shrestha, T.; Basirat, M.; Charit, I.; Potirniche, G.P.; Rink, K.K. Creep rupture behavior of Grade 91 steel. *Mater. Sci. Eng. A* **2013**, *565*, 382–391.
9. Ahn, J.C.; Sim, G.M.; Lee, K.S. Effect of aging treatment on high temperature strength of Nb added ferritic stainless steels. *Mater. Sci. Forum* **2005**, *475*, 191–194.
10. Ganesh, B.J.; Raju, S.; Rai, A.K.; Mohandas, E.; Vijayalakshmi, M.; Rao, K.B.S.; Raj, B. Differential scanning calorimetry study of diffusional and martensitic transformations in some 9 wt-% Cr low carbon ferritic steels. *Mater. Sci. Technol.* **2011**, *27*, 500–512.
11. Yoshino, M.; Mishima, Y.; Toda, Y.; Kushima, H.; Sawada, K.; Kimura, K. Influence of normalizing heat treatment on precipitation behavior in modified 9Cr-1Mo steel. *Mater. High Temp.* **2008**, *25*, 149–158.
12. Totemeier, T.C.; Tian, H.; Simpson, J.A. Effect of normalization temperature on the creep strength of modified 9Cr-1Mo steel. *Metall. Mater. Trans.* **2005**, *37*, 1519–1525.

13. Dudko, V.; Delyakov, A.; Kaibyshev, R. Effect of tempering on mechanical properties and microstructure of a 9% Cr heat resistant steel. *Mater. Sci. Forum* **2012**, *706*, 841–846.

14. Sawada, K.; Suzuki, K.; Kushima, H.; Tabuchi, M.; Kimura, K. Effect of tempering temperature on Z-phase formation and creep strength in 9Cr-1Mo-V-Nb-N steel. *Mater. Sci. Eng. A* **2008**, *480*, 558–563.

15. Masuyama, F.; Nishimura, N. Experience with creep-strength enhanced ferritic steels and new emerging computational methods In Proceedings of the 2004 ASME/JSME Pressure Vessels and Piping Conference, San Diego, CA, USA, 25–29 July 2004; Volume 476, pp. 85–92.

16. Shen, Y.Z.; Kim, S.H.; Cho, H.D.; Han, C.H.; Ryu, W.S. Identification of precipitate phases in a 11Cr ferritic/martensitic steel using electron microdiffraction. *J. Nucl. Mater.* **2010**, *400*, 64–68.

17. Anderson, P.; Bellgard, T.; Jones, F.L. Creep deformation in a modified 9Cr-1Mo steel. *Mater. Sci. Technol.* **2003**, *19*, 207–213.

18. Das, C.R.; Albert, S.K.; Bhaduri, A.K.; Srinivasan, G.; Murty, B.S. Effect of prior microstructure and mechanical properties of modified 9Cr-1Mo steel weld joints. *Mater. Sci. Eng. A* **2008**, *477*, 185–192.

19. Silwal, B.; Li, L.; Deceuster, A.; Griffiths, B. Effect of post-weld heat treatment on toughness of heat-affected zone of Grade 91 steel. *Welding J.* **2013**, *92*, 80s–87s.

20. Shtansky, D.V.; Inden, G. Phase transformation in Fe-Mo-C and Fe-W-C steels—II. Eutectoid reaction of M23C6 carbide decomposition during austenitization. *Acta Mater.* **1997**, *45*, 2879–2895.

21. Ganesh, B.J.; Raju, S.; Mohandas, E.; Vijayalakshmi, M. Effect of thermal aging on the transformation temperatures and specific heat characteristics of 9Cr-1Mo ferritic steel. *Defect Diffus. Forum* **2008**, *279*, 85–90.

22. Oono, N.; Nitta, H.; Iijima, Y. Diffusion of Nb in α-iron. *Mater. Trans.* **2003**, *44*, 2078–2083.

23. Raju, S.; Ganesh, B.J.; Rai, A.K.; Saroja, S.; Mohandas, E.; Vijayalakshmi, M.; Raj, B. Drop calorimetry studies on 9Cr-1W-0.23V-0.06Ta-0.09C reduced activation steel. *Int. J. Thermophys.* **2010**, *31*, 399–415.

24. Hald, J.; Korcakova, L.; Danielsen, H.K.; Dahl, K.V. Thermodynamics and kinetic modeling: Creep resistant materials. *Mater. Sci. Technol.* **2009**, *24*, 149–158.

25. Hong, S.G.; Jun, H.J.; Kang, K.B.; Park, C.G. Evolution of precipitates in the Nb-Ti-V microalloyed HSLA steels during reheating. *Scr. Mater.* **2003**, *48*, 1201–1206.

26. Taylor, K.A. Solubility products of titanium-, vanadium-, and niobium-carbide in ferrite. *Scr. Mater.* **1995**, *32*, 7–12.